

Phase Transition and Electronic Structure Investigation of MoS₂-rGO Nanocomposite Decorated with AuNPs.

Yunier Garcia-Basabe^{1,*}, Gabriela F. Peixoto², Daniel Grasseschi^{2,3}, Eric C. Romani⁴, Flávio C. Vicentin⁵, Cesar E. P. Villegas⁶, Alexandre. R. Rocha⁷ and Dunieskys G. Larrude³

¹ Universidade Federal da Integração Latino-Americana, UNILA, 85867-970, Foz do Iguaçu, Brazil.

² Inorganic Chemistry Department, Chemistry Institute, Federal University of Rio de Janeiro (UFRJ), 21941-909, Rio de Janeiro, Brazil

³ MackGraphe-Graphene and Nanomaterial Research Center, Mackenzie Presbyterian University, 01302-907, São Paulo, Brasil.

⁴ SENAI Innovation Institute for Virtual Production Systems, 20911-210, Rio de Janeiro, Brazil.

⁵ Brazilian Synchrotron Light Laboratory (LNLS), Brazilian Center for Research in Energy and Materials (CNPEM), 13083-970, Campinas, Sao Paulo, Brazil.

⁶ Departamento de Ciencias, Universidad Privada del Norte, Av. Andrés Belaunde Cdra. 10 s/n, 15324, Comas, Lima, Peru.

⁷ Instituto de Física Teórica, State University of São Paulo (UNESP), 01049-010, São Paulo, Brazil.

*Corresponding Author:

Prof. Dr. Yunier Garcia-Basabe

E-mail address: yunier.basabe@unila.edu.br and yunierbasabe26@gmail.com

ORCID iD: 0000-0001-5683-0108

.Keywords: MoS₂, Reduced graphene oxide, nanocomposite, phase transition, electronic structure, surface decoration, gold nanoparticles

ABSTRACT

In this work a simple approach to transform MoS₂ from its metallic (1T' to semiconductor 2H) character via gold nanoparticle surface decoration of a MoS₂ graphene oxide (rGO) nanocomposite is proposed. The possible mechanism to this phase transformation was investigated using different spectroscopy techniques, and supported by density functional theory theoretical calculations. A mixture of the 1T'- and 2H-MoS₂ phases was observed from the Raman and Mo 3d High Resolution X-ray photoelectron (HRXPS) spectra analysis in the MoS₂-rGO nanocomposite. After surface decoration with gold nanoparticles the concentration of the 1T' phase decreases making evident a phase transformation. According to Raman and valence band spectra analyses, the AuNPs induces a p-type doping in MoS₂-rGO nanocomposite. We proposed as a main mechanism to the MoS₂ phase transformation the electron transfer from Mo 4d_{xy,xz,yz} in 1T' phase to AuNPs conduction band. At the same time, the unoccupied electronic structure was investigated from S *K*-edge Near Edge X-Ray Absorption Fine Structure (NEXAFS) spectroscopy. Finally, the electronic coupling between unoccupied electronic states was investigated by the core hole clock approach using Resonant Auger spectroscopy (RAS), showing that AuNPs affect mainly the MoS₂ electronic states close to Fermi level.

1 INTRODUCTION

Over the past few years, two-dimensional transition metal dichalcogenides (TMDs) have become attractive options for electronic devices, transistors, biosensors, as well as for applications in catalysis and energy storage devices [1-3]. Among the TMD family MoS_2 is the most investigated due to its unique physical and chemical properties [4,5]. A singular feature of MoS_2 layered materials is the structural polymorphism, which modulates its electronic structure. In particular, the 2H and 1T phases with different arrangement of the S and Mo atoms have been reported for MoS_2 crystals [6]. The 2H- MoS_2 is the most stable structure, where each layer is constructed from the Mo atom sandwiched between two S atoms in a trigonal prismatic (D_{3h}) geometry. On the other hand, the 1T- MoS_2 phase is based on Mo atoms octahedrally (O_h) coordinated to S atoms. MoS_2 in 1T phase is metastable (easily converted to the stable 2H phase) while in the octahedral distorted configuration (1T') it turns into a phase that is thermodynamically stable [7]. The trigonal prismatic symmetry in 2H- MoS_2 induces a semiconductor electronic structure with monolayer direct band gap of ~ 1.8 eV, [1,8] while the octahedral coordination of the Mo atoms in the 1T'- MoS_2 phase gives rise to a metallic behavior with good conductivity [1,9]. Recently, several works about the physical and chemical treatment of MoS_2 to obtain a reversible transition between these two phases have been reported [6,10-12]. In most of them, the 1T'- MoS_2 phase presents superior electrocatalytic properties, while 2H- MoS_2 is an excellent candidate for optoelectronic applications [13-15].

While isolated MoS_2 has attractive properties, the formation of MoS_2 -graphene nanocomposites could be an excellent approach to improve its performance for different device applications [16-20] as the mechanical flexibility, electronic conductivity and

chemical stability of graphene could be added to the properties of isolated MoS₂. Recently it was reported that p-MoS₂/n-rGO nanocomposites have better photocatalytic activity in hydrogen generation when compared to pristine MoS₂ [21,22]. At the same time noble metal nanoparticles (NPs) decorating the MoS₂-graphene nanocomposite surface could potentially extend its functionalities as novel catalytic, magnetic, and optoelectronic nanomaterials even further [2,23-26]. Among these nanoparticles, Gold (AuNPs) is of special interest due to their non-toxicity and excellent stability. In fact, Au-MoS₂ composite synthesis, electrical and thermal properties and its application on photocatalytic water splitting and hydrogen production has been the subject of a number of works [27-31].

Nevertheless, the knowledge of the electronic structure of the MoS₂-graphene nanocomposites is a crucial piece of information for better understanding their biosensing, photonics, catalytic and optoelectronic device performance. In particular, controlling the different phases with metallic and semiconductor behavior of the nanocomposite is of utmost importance for appropriately tailoring properties, and subsequent applications. In this sense, in the present work, the effect of AuNPs decoration on the stability of MoS₂ (1T' and 2H) phases and in the electronic structure of a MoS₂-rGO nanocomposite was investigated. The local electronic structure of either the pristine nanocomposite, and decorated with AuNPs was studied using High Resolution X-ray Photoelectron Spectroscopy (HRXPS), Near Edge X-Ray Absorption Fine Structure (NEXAFS), Resonant Auger Spectroscopy (RAS), and Density Functional Theory simulations (DFT). The non-local electronic structure was investigated by Valence band and Raman spectra. A mixture of the 1T' and 2H phases of MoS₂ was observed from the Raman spectrum in the solvothermal-synthesized MoS₂-rGO nanocomposite and corroborated from Mo 3d HRXPS spectra analysis. A

decrease of the Mo^{4+} (1T') species is shown after surface decoration with AuNPs, making evident a phase transformation from 1T' to 2H-MoS₂. We identify surface electron transfer processes from MoS₂-rGO to AuNPs as the main mechanism for this phase transformation using Raman and XPS valence band spectra analysis. At the same time, the unoccupied electronic structure was investigated from S K-edge NEXAFS spectroscopy. The degree of delocalization and/or electronic coupling between unoccupied electronic states was investigated by the core hole clock approach showing that AuNPs affect the electronic states close to the Fermi level.

2. EXPERIMENTAL DETAILS

2.1 Synthesis procedure

Graphene oxide synthesis was carried out by a modified Hummers method in a calorimetric automated reactor. 0.75 g of pristine graphite flakes (Aldrich) was added to 90 mL of sulfuric acid (Sigma-Aldrich) and 10 mL of phosphoric acid followed by the slow addition of 4.5 g of potassium permanganate. This system was kept under stirring for two hours at 50°C. Subsequently, the temperature was decreased to 0°C then poured on 400 mL of ice, followed by 2 mL of hydrogen peroxide (30 vol% on water, Sigma-Aldrich). The solid material was purified by centrifugation and washed with different amounts of water, hydrochloric acid solution (10 vol%), ethanol, acetone and DI water again. The black and solid material (Graphite oxide – Gr-O) was dried under vacuum overnight. An aqueous suspension of graphite oxide was then sonicated (50W, 40 kHz) in DI water for 2 min. The resulting brown and stable suspension was found to be Graphene Oxide.

For the preparation of MoS₂-rGO nanocomposite, 25 mg of (NH₄)₂MoS₄ was added to 10 mg of graphene oxide (GO) dispersed in 10 mL of dimethylformamide (DMF). The mixture was sonicated at room temperature for approximately 10 min until a clear and homogeneous solution was achieved. After that, 0.1 mL of N₂H₄•H₂O was added. The reaction solution was further sonicated for 30 min before transferred to a 150 mL Teflon-lined autoclave. The autoclave was sealed and heated in an oven at 200 °C for 10 h. The product was collected by centrifugation at 8000 rpm for 5 min and resuspended in DI water. This washing process was repeated 5 times to remove the DMF.

Gold nanoparticles were synthesized according the procedure described by Grasseschi et al [32]. All glassware were previously cleaned with aqua regia ($3\text{HCl}:1\text{HNO}_3$), in order to prevent any possible influence of contaminants in gold reduction process. The synthesis was performed, by heating 50 mL of gold solution HAuCl_4 solution ($5.08 \times 10^{-4} \text{ mol L}^{-1}$) in a 125 mL round bottom flask, and refluxing, using a computer controlled system, for keeping the temperature ($\pm 1^\circ\text{C}$) and stirring rates constants. Then, 1.7 mL of aqueous sodium citrate solution (0.038 mol L^{-1}) was added dropwise ($100 \mu\text{L s}^{-1}$), while the mechanical stirring and temperature were kept constant, at 1150 rpm and 95°C , respectively. After 5 min, the solution was cooled to room temperature.

A simple method was utilized to obtain the $\text{MoS}_2\text{-rGO-AuNPs}$ nanocomposite. Thin film of $\text{MoS}_2\text{-rGO}$ was deposited on the SiO_2/Si substrate by the drop casting method. After that, two drops of $25\mu\text{L}$ of the AuNPs solution were deposited to cover the entire film surface. The sample was dried in air at room temperature for 24 h.

2.2 Characterization

In order to obtain morphological information of the samples, transmission electron microscopy (TEM, JEOL JEM 2100), Scanning transmission electron microscopy (STEM) using a high angular dark field detector (HAADF, FEI Titan 80-300) and Scanning electron microscopy (SEM, JEOL JSM-7800F and Phenom ProX) were performed. The Raman spectra were collected using a WITec Alpha 300R confocal Raman imaging microscope using a laser line centered at 532 nm and 0.508 mW of power. For reducing the sample locations effect, the Raman spectra in both samples were collected at four different points and the reproducibility of results were observed. X-ray photoelectron spectroscopy (XPS) (K-Alpha Thermo Scientific)

measurements and analyses were conducted to investigate the local electronic structure of the chemical species on MoS₂-rGO and MoS₂-rGO-AuNPs nanocomposites. The monochromatized Al K α ($h\nu=1486.6$ eV) excitation energy with 400 μm X-ray spot size was used for XPS measurements. The electron energy analyzer was operated at constant pass energy of 25 eV, and 200 eV for high resolution (HR) and survey spectra, respectively. An instrumental energy resolution of 0.25 eV determined from Ag_{5/2} peak from pure silver was used for HRXPS experiments. A flood gun source of low energy electrons and Ar⁺ ions was used during all measurements in order to prevent surface charging. The high-resolution XPS spectra were processed using Thermo Scientific's Advantage XPS software package (version 4.61) and using a linear combination of Gaussian and Lorentzian line shapes for the spectra fitting, with a Shirley function for background correction. The binding energy scale was calibrated by attributing an energy value of 284.5 eV to C-C/C-H species in HR C1s spectrum.

The electronic structure for unoccupied states was investigated from X-ray absorption (XAS) and Resonant Auger (RAS) spectroscopies experiments. XAS and RAS were measured at the soft X-ray spectroscopy (SXS) beamline at the Brazilian Synchrotron Light Source (LNLS) facilities [33]. A Si(111) double-crystal monochromator in high resolution condition with energy bandwidth of 0.48 eV was used to cover Sulphur K-edge. Near Edge X-Ray Absorption Fine Structure spectra were recorded in the total electron yield mode (TEY). The final data was normalized by this photon flux spectrum (estimated from Au mesh) to correct the fluctuations in beam intensity. Presented spectra are averages from at least three scans, background corrected by a linear pre-edge subtraction and linear regression beyond the edge. Multiple-scan RAS spectra were collected inside an ultrahigh vacuum chamber (UHV) with a base pressure of 10⁻⁹ mbar using a hemispherical electron energy analyzer (Specs model phoibos 150) with 45°

take-off direction of Auger electrons and 25 eV of pass energy. The total energy resolution was 0.76 eV. RAS spectra fittings were performed using Pseudo-Voigt profile functions (linear combination of Gaussian (G) and Lorentzian (L) functions) and the background was corrected using a Shirley function.

2.3 Theoretical Simulations

Plane-wave density functional theory [34,35] was used to obtain the electronic ground-state using the Perdew-Burke-Ernzerhof (PBE) generalized gradient exchange-correlation functional, [36] implemented in the Quantum-Espresso (QE) package, [37] and Non-empirical van der Waals corrections proposed by Tkachenko and Scheffler [38] were included in all calculation. The kinetic energy cutoff was set to 90 Ry and a mesh of 14 x 14 x 1 k-points in the Monkhorst-Pack scheme was used. The structures were fully optimized to their equilibrium positions with forces smaller than 0.01 eV/Å. A vacuum region of 15 Å was used to suppress the coupling between neighboring slabs. The interfaces were modeled by choosing an Au (111) surface with 4 atomic layers. Subsequently a fully relaxed 1T'-MoS₂ (2H-MoS₂) monolayer is adsorbed on the Au(111) surface following the arrangement proposed by Zhou et al [39]. By doing this, both the Au(111) and 2H-MoS₂ unit cell is matched with the ideal lattice constant of 1T'-MoS₂ monolayers. We should mention that this five-layer model has been adopted in previous works describing well some features observed in experiments [40,41].

3. RESULTS AND DISCUSSION

The morphology of the MoS₂-rGO and MoS₂-rGO-AuNPs nanocomposites were characterized by SEM, TEM e STEM microscopy images and are depicted in Figure 1. . As seen in SEM (Figure 1a), TEM (Figure 1b) and STEM (Figure 1c) images, the MoS₂-rGO nanocomposite consist of MoS₂ layer covering the surface of the rGO sheets. MoS₂ basal planes are clearly observed from high magnification TEM image shown in Figure 1b. Moreover, the HRTEM image reveals a large number of MoS₂ layers with interlayer distance of 0.62 nm (corresponding to the (002) plane) stacked together. Energy dispersive X-ray spectra (EDX) (Figure 1g and Figure S1 on the Supporting Information File (SI)) shows that Mo, S, C and O elements were distributed uniformly on the entire flake. Some regions show the formation of spherical particles of MoS₂ with an average diameter of approximately a hundred nanometers covering the rGO surfaces (Figure S1).

The effect of AuNPs decorating the MoS₂-rGO surface is presented in Figure 1d, showing a substantial coverage of AuNPs (bright points) in the surface of the MoS₂ and promoting the formation wrinkled nanosheets. The TEM and STEM images on Figure 1e and f show that the AuNPs are spherical with an average size of 23.5 ± 3.5 nm with good size dispersion, as indicated by the size distribution on Figure 1h. The EDX spectra record at different points (Figure 1g and Figure S1 and S2) confirm the presence of gold on the MoS₂-rGO surface.

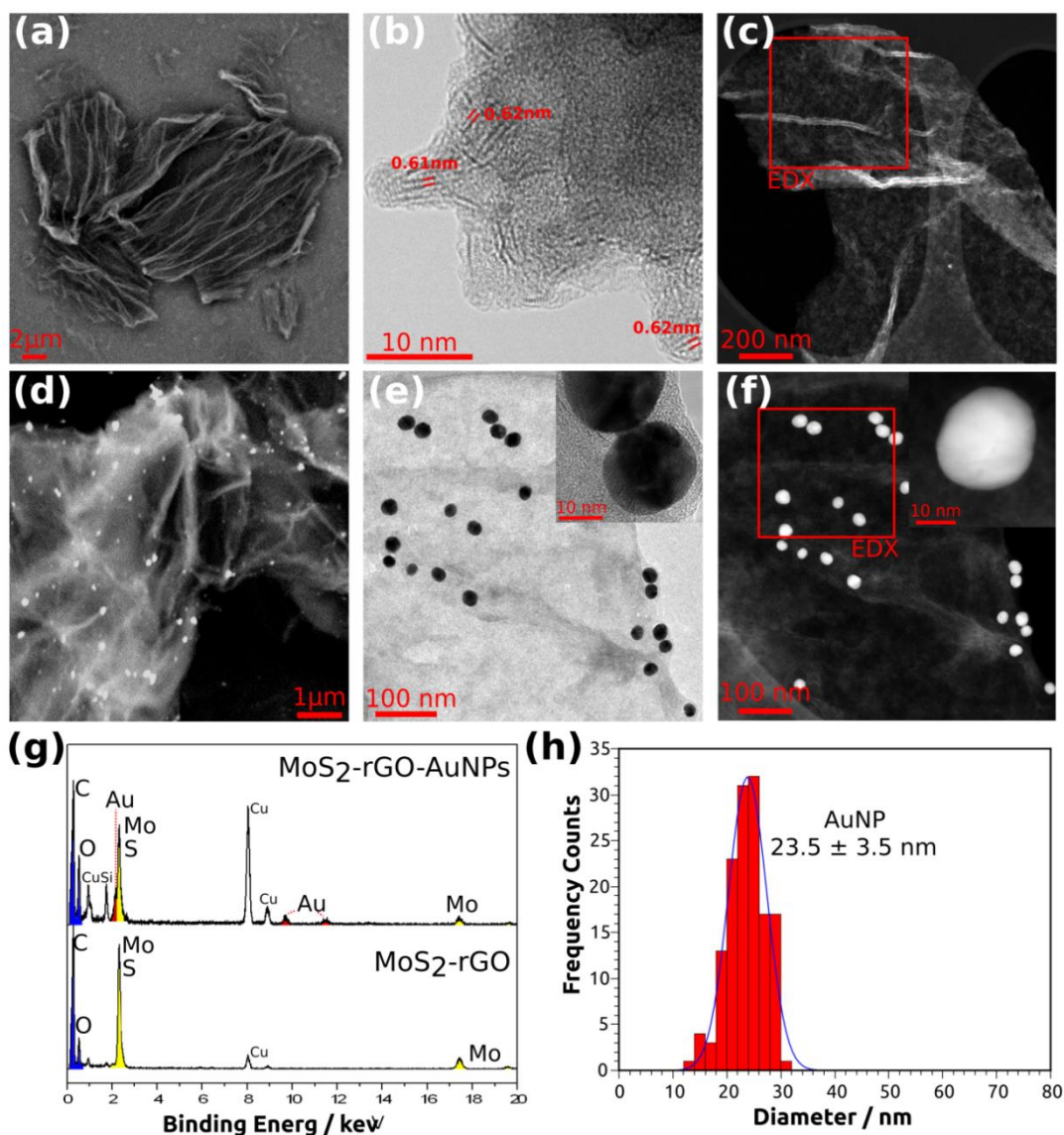


Figure 1. SEM images of MoS₂-rGO (a) and MoS₂-rGO-AuNPs (d) nanocomposites. TEM images of MoS₂-rGO (b) and MoS₂-rGO-AuNPs (e) nanocomposites. STEM - HAADF images of MoS₂-rGO (c) and MoS₂-rGO-AuNPs (f) nanocomposite. EDX spectra of MoS₂-rGO and the MoS₂-rGO-AuNPs nanocomposites of the selected areas on c and f (g). AuNPs size distribution (h).

Figure 2 shows the Raman spectra of MoS₂-rGO and MoS₂-rGO-AuNPs nanocomposites. These spectra exhibit the D, G and D' peaks, vibrational modes characteristic of graphitic materials [39,42]. The G-band corresponds to the in-plane optical mode due to bond stretching of graphitic sp² carbon atoms. The D-band originates from the lattice defect and lattice distortion, while D'-band is attributed to

inter and intra-valley scattering processes. The three peaks observed at 327, 379.1 and 407 cm^{-1} (Figure. 2(b)) correspond to the in-plane E_{1g} and E_{2g}^1 and out-plane A_{1g} vibrational modes of the 2H-MoS₂, respectively [42-44]. The A_{1g} peak position and the A_{1g} - E_{2g}^1 frequency difference ($\sim 28 \text{ cm}^{-1}$) point to the formation of few-layer MoS₂ with more than 5 layers [45]. A blue shift of about ~ 1 and 4 cm^{-1} (Fig. 2(c)) after AuNPs surface decoration were observed for E_{2g}^1 and A_{1g} Raman modes of MoS₂, respectively. The last behavior is an indicative of involvement of charge transfer processes between MoS₂-rGO sheets and dispersed AuNPs, more specifically a p-type doping, where electrons are transferred from MoS₂-rGO to AuNPs [46]. Other three peaks at 150, 218 and 328 cm^{-1} , attributed to the J_1 , J_2 and J_3 longitudinal acoustic modes of S-Mo-S bonds in 1T'-MoS₂ phase, are characterizing the Raman spectrum of the MoS₂-rGO nanocomposite (Figure 2(b)). Demonstrating the coexistence of 1T' and 2H phases in this sample [7,47]. The coexistence of this two phase in MoS₂-rGO nanocomposite was also reported by Jeffery et al., showing that 1T' phase stability is associated to rGO content [48]. After AuNPs surface decoration the intensity of J_1 , J_2 and J_3 peaks of 1T' phase becomes much weaker, while the A_{1g} peak (typical of 2H-MoS₂ phase) becomes more intense. This result is an indication of phase transformation from metallic 1T' to the semiconducting 2H-MoS₂ phase with the presence of AuNPs. The metallic to semiconductor transformation in MoS₂-rGO nanocomposite after AuNPs surface decoration could be a promising approach to keep the light absorbing properties of MoS₂ with a good electrical conductivity, mechanical stability and high surface area due to the presence of rGO support, making this material an excellent candidate for optoelectronic devices and photocatalytic applications.

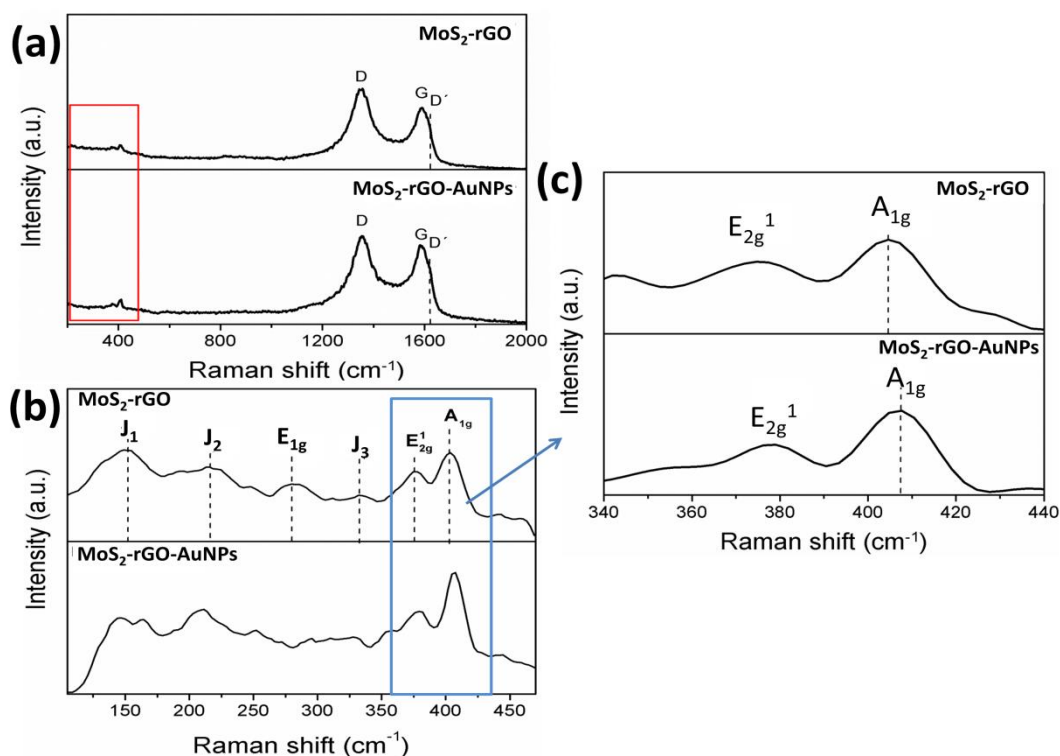


Figure 2. (a) Raman spectra of the MoS₂-rGO and MoS₂-rGO- AuNPs nanocomposites. (b) Raman spectra showing the MoS₂ peak regions (inside of red rectangle in figure (a)). (c) Raman spectra showing E_{2g}¹ and A_{1g} vibrational modes (inside of blue rectangle in figure (b)).

The chemical composition of the MoS₂-rGO and MoS₂-rGO-AuNPs nanocomposites was estimated from survey XPS spectra as shown in Figure 3. The core level Mo 3d, S2p, C1s and O1s peaks found in the spectrum of MoS₂-rGO confirm the presence of the constituent elements in this nanocomposite. Additionally, Au 4f core level doublet peaks (Au 4f_{7/2} at 84.1 eV and Au 4f_{5/2} at 87.8 eV shown in Figure S3) are observed for the MoS₂-rGO-AuNPs sample, confirming the presence of gold nanoparticles in metallic state decorating the MoS₂-rGO surface. The atomic percentages for each nanocomposite are reported on Table 1. The S/Mo atomic ratio of ~2, close to the theoretical stoichiometry formula of MoS₂ is found for pristine MoS₂-rGO. However, a significant decrease (from 17.1% in pristine MoS₂-rGO to 8.3% in MoS₂-rGO-AuNPs) in the S content is observed after AuNPs surface decoration. The

last result may be associated to the fact that the AuNPs on the MoS₂-rGO surface are adsorbed on top of the S atoms sites. This result is in agreement with previous theoretical reports where was found that Au adatom favors to adsorb at the top of S atom and with a strong hybridization between the *s* orbital of Au and the Mo 4d states [49,50]. A slight increase of C and O species content is also observed in the MoS₂-rGO-AuNPs sample compared with the pristine case, which can be associated to the presence of citrate ligands utilized to stabilize the AuNPs in solution [32].

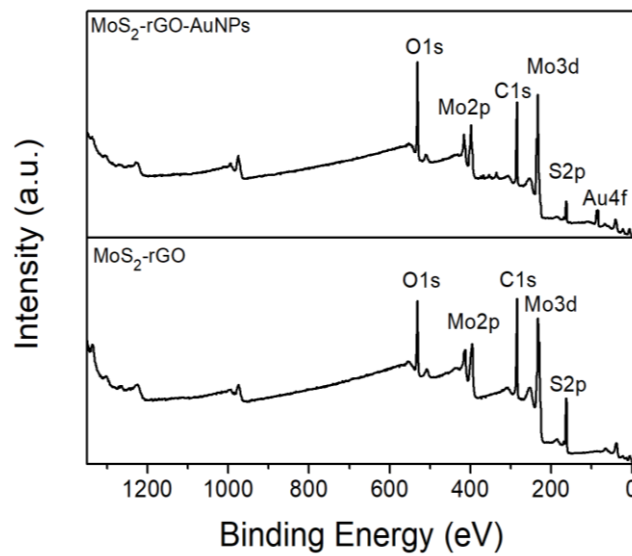


Figure 3. XPS survey spectra of MoS₂-rGO and MoS₂-rGO-AuNPs nanocomposites.

Table 1. Surface chemical composition (at.%) distribution of MoS₂-rGO and MoS₂-rGO-AuNPs nanocomposite films obtained from XPS survey spectra analysis.

	C1s	O1s	Mo3d	S2p	Au4f
MoS ₂ -rGO	55.4	19.6	7.8	17.1	-
MoS ₂ -rGO-AuNPs	57.5	24.4	9.0	8.3	0.73

AuNPs doping effects in the stability of MoS₂ (1T' and 2H) phases and in the local electronic structure for the MoS₂-rGO nanocomposite were investigated with high resolution XPS spectra analysis. Figure 4 shows the C1s, S2p, Mo 3d and O1s high

resolution XPS spectra of both nanocomposites. The fitting parameters, (Binding Energy - BE), full width at half maximum (FWHM) and species amount (% area) of high resolution spectra are summarized in the Table S1. The high resolution C1s XPS spectra of both nanocomposites showed in Figure 4(a) were deconvoluted using three components: peak at BE=284.5 eV can be attributed to C-C/C=C sp^2 carbon species, the peak at BE=285.9 eV can be attributed to hydroxyl carbon C-O, and the peak at BE=288.2 eV carboxylate carbon O-C=O [25]. These spectra are similar to the C1s XPS spectrum of isolated rGO reported in the literature [25,28]. There are no significant differences between the C1s XPS spectrum of MoS₂-rGO before and after the decoration with AuNPs.

Three sulphur species with their respective spin-orbital doublets are observed in the S2p XPS spectra of both nanocomposites (Figure 4(b)). The peaks at BE = 161.8 eV and 163.1 eV correspond to the S 2p_{3/2} and 2p_{1/2} sulfur species in MoS₂ [51-53]. The second S species observed in the S2p region was attributed to bridging C-S-C structures (BE = 163.3 eV and 164.4 eV to the S 2p_{3/2} and 2p_{1/2}, respectively) [35]. The high energy component at BE = 168.5 eV (S 2p_{3/2}) can be associated to S⁶⁺ species in C-SO_x-C sulfate groups [52,53].

More representative differences between the electronic structure of MoS₂-rGO and MoS₂-rGO-AuNPs nanocomposites are observed in the high resolution Mo 3d and O1s XPS spectra. According to previous reports the diverse electronic properties of TMDs arise from the progressive filling of the non-bonding d bands [54,55]. The effect of chalcogen atoms on the electronic structure is minor compared with that of the metal atoms, since the top of the valence band has higher contribution from the Mo orbitals. The phase stability of TMDs also depends of the effective change in the d-electron count in the transition metal atom.

The Mo 3d XPS spectrum of MoS₂-rGO nanocomposite is characterized by four contributions associated to different oxidization states and structural phases of the Mo species in this nanocomposite (Figure 4(c)). The peaks at BE = 230.0 eV and 233.2 eV correspond to Mo⁴⁺ 3d_{5/2} and Mo⁴⁺ 3d_{3/2} components of 2H-MoS₂ (2H) phase of MoS₂. The deconvolution of the Mo 3d spectrum identified additional peaks (Mo⁴⁺ 3d_{5/2} at 229.0 eV and Mo⁴⁺ 3d_{3/2} 232.1 eV) appearing at BE ~1 eV below of the corresponding peaks of the 2H phase which were attributed to 1T'-MoS₂ phase [10,51,52,56-60]. The peaks at 231.2 and 234.4 eV, with separation energy of 3.2 eV, can be attributed to the Mo 3d_{5/2} and Mo 3d_{3/2} due to the presence of Mo⁵⁺ [43,53]. In the high energy region of the spectrum, the Mo 3d_{5/2} (232.7 eV) and Mo 3d_{3/2} (235.8 eV) peaks associated to Mo⁶⁺ can be found [52, 53]. The peak at BE = 226.3 eV in the low energy region of the Mo 3d spectrum corresponds to S2s contribution. The Mo3d HRXPS results are in accordance with the Raman discussion, showing that MoS₂-rGO nanocomposite is composed of a mix of 1T' and 2H MoS₂ phases. The same Mo chemical species are observed for the MoS₂-rGO-AuNPs sample; however, some important differences are seen concerning their content after AuNPs surface decoration. We notice an increase of Mo⁶⁺ oxidation species, while the Mo⁴⁺ (1T')/ Mo⁴⁺(2H) ratio decreases from 1.7 to 0.6 after the decoration of the MoS₂-rGO surface with Au nanoparticles. The increase of Mo⁶⁺ and the decrease of Mo⁴⁺ (1T'-MoS₂) can be interpreted as electron transfer from MoS₂-rGO to Au NPs, converting the MoS₂-rGO electronic structure from a metallic to a semiconductor character, corroborating with our Raman spectroscopy results. The increment of Mo⁶⁺ in MoS₂ after AuNPs decoration was also reported by Kim et al. and was attributed to oxidation of MoS₂ to molybdic acid [61].

The high resolution O1s spectrum (Figure 4(d) bottom) was deconvoluted by three peaks at BE= 530.6, 531.7 and 533.1eV, respectively. These contributions are

associated with C-C=O, C=O/-COOH and OH groups, respectively. After decorating the MoS₂-rGO surface with AuNPs, the OH species disappear, which may be attributed to a reduction of the surface adsorbed oxygen (water).

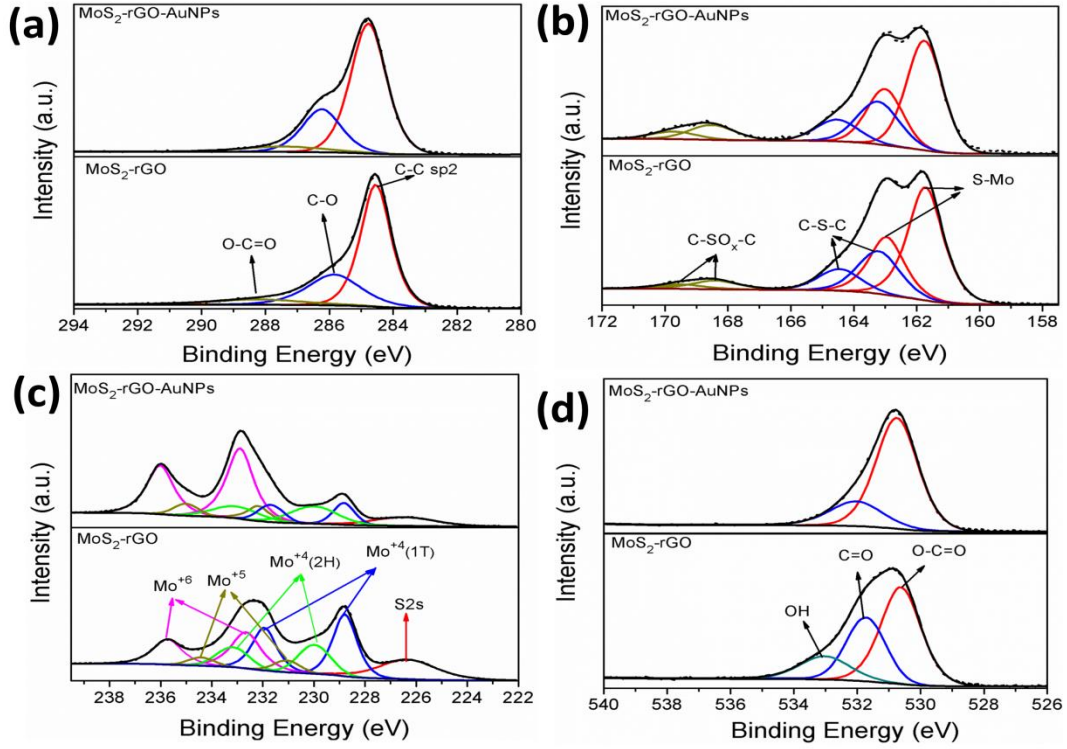


Figure 4. High resolution XPS spectra of MoS₂-rGO and MoS₂-rGO-AuNPs nanocomposites: (a) C1s, (b) S2p, (c) Mo 3d and (d) O1s core levels.

To elucidate the mechanism that induces the phase transition in the nanocomposite, DFT calculations were performed on the different MoS₂ phases with or without the presence of gold. It has been proposed that a phase transition can be induced by charge transfer to the TMD [58]. According to Gao, et al., electron injection can stabilize the 1T'-MoS₂ phase [58]. However, our experimental results show that electrons are transferred from the MoS₂ to the AuNPs reducing the stability of the 1T'-phase and enabling the transition to the more stable 2H-MoS₂. We looked at the effects of the interaction between Au and MoS₂ in the electronic structure (Figure 5(b)). For the 2H phase adsorbed on an Au (111) surface (see Figure S4) we note little or no effect on

the band structure of MoS₂ compared to the isolated case. On the other hand, for the 1T'-phase - which is metallic - there is a strong interaction between the metal and the monolayer of MoS₂, particularly around the G and M points of the spectrum where the band character becomes intertwined between gold and the TMD indicating a stronger interaction which favors the electrons transfers between the AuNPs and MoS₂.

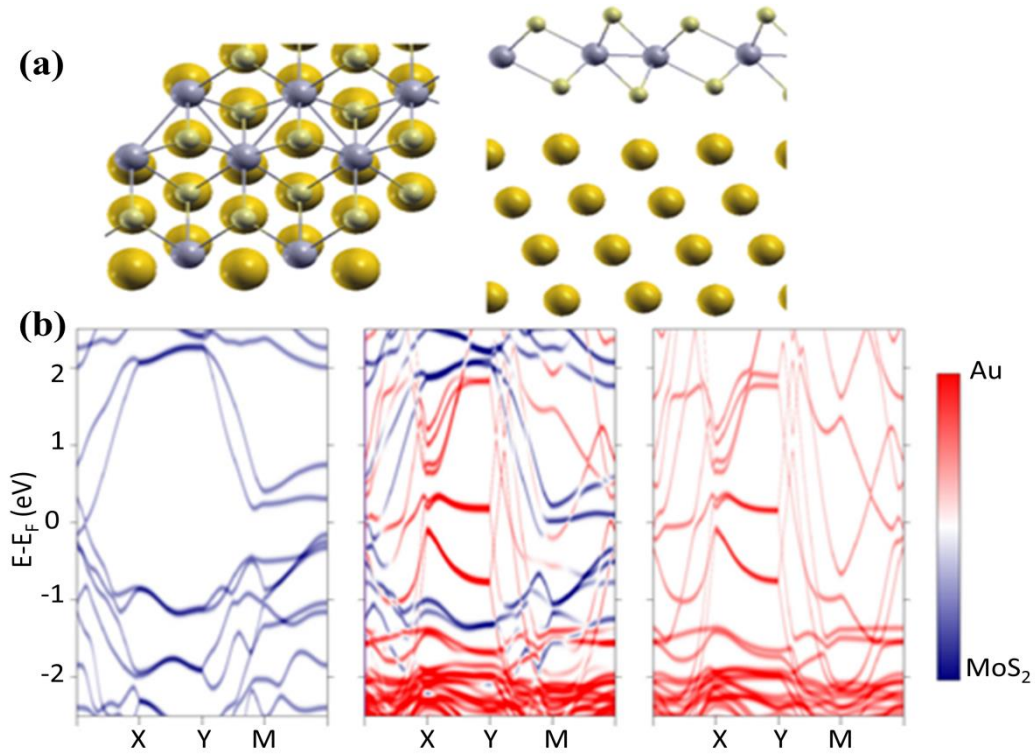


Figure 5. (a) Top and lateral view of the 1T' phase of MoS₂ adsorbed on a gold (111) surface. (b) Band structure projected on orbitals of the different constituents for the isolated (1T'-MoS₂ and Au (111)) structures (outer panels), and the composite material (inner panel).

The valence band (VB) XPS spectra of MoS₂-rGO and MoS₂-rGO-AuNPs nanocomposites are shown in Figure 6. The valence band spectrum for MoS₂-rGO is qualitatively similar to MoS₂ stemming from the hybridization of Mo4d and S3p electronic states [61]. According to crystal-field theory, Mo 4d orbitals are split into three orbitals (see the Figure 6(c)): one with low energy $4d_{z^2}$ 4d, two doubly degenerated composed by $4d_{x^2-y^2,xy}$ 4d(empty) and two doubly degenerated $4d_{xz,yz}$ (empty) for 2H-MoS₂ phase (in hexagonal D_{3h} configuration). In this case Mo $4d_{z^2}$ is fully occupied by two spin paired electrons forming the VB. However, 1T'-MoS₂ (octahedral O_h (1T')) is composed by three degenerated orbitals $4d_{xy, xz,yz}$ and doubly degenerated $4d_{x^2-y^2,z^2}$ VB in 1T'-MoS₂ is composed by partially occupied $4d_{xy,xz,yz}$ [61, 62]. The main effect of AuNPs surface decoration is observed through the decreasing of the peak at ~ 2 eV, close to valence band edge. This behavior can be associated to an electron transfer from Mo 4d states to AuNPs conduction band how was depicted from Mo3d HRXPS and Raman spectra analyzed previously. Therefore, after a careful analysis of the valence band region and from theoretical calculations by DFT, comparing the electronic coupling between Au and MoS₂ states for 1T' and 2H phases (Figure 5(b) and Figure S4) we can conclude that a possible mechanism for the phase transformation from 1T' to 2H-MoS₂ that arises after surface decoration is the output of electrons specifically from the Mo $4d_{xy,xz,yz}$ that make up the VB in phase 1T'.

Figure 6(b) shows the extrapolation procedure to determine the valence band maximum edge for both nanocomposites from valence band XPS spectra. A shift ~ 0.1 eV to lower BE values is observed after nanoparticle decoration. This shift is an indicative of p-type doping, where the AuNPs behave as electron acceptors from MoS₂-rGO valence band [61,62]. This result is in agreement with Mo3d XPS analysis where the electron transfer from MoS₂-rGO to AuNPs decreased their metallic character.

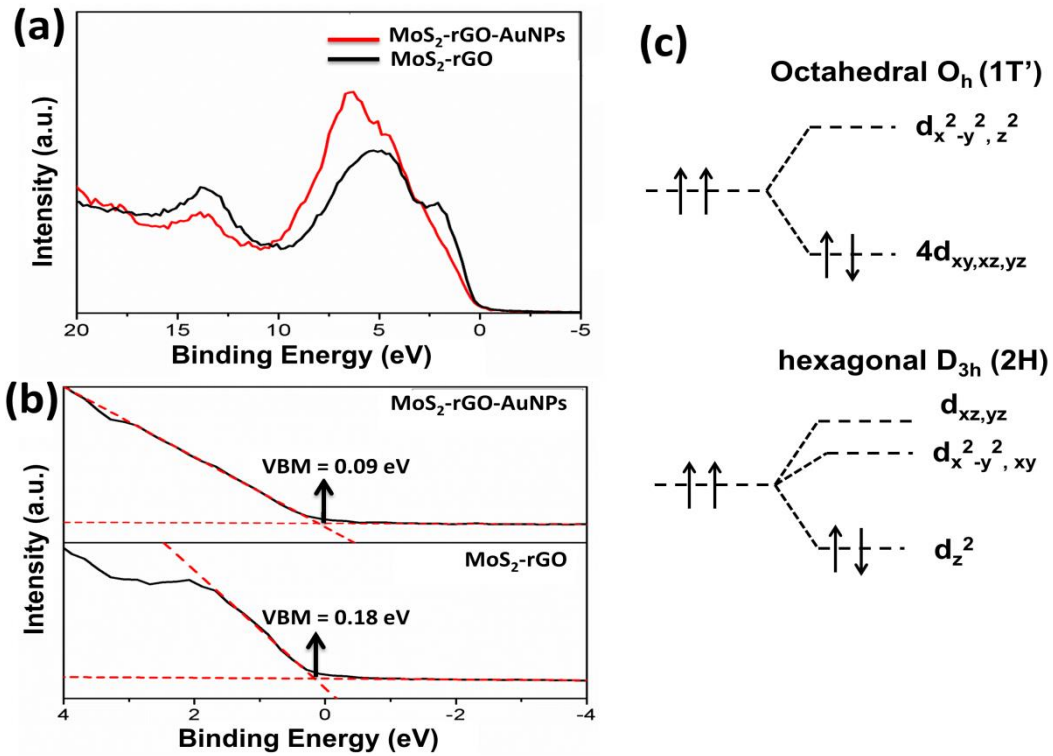


Figure 6. (a) Valence band XPS spectra of MoS₂-rGO and MoS₂-rGO-AuNPs nanocomposites. (b) Extrapolation procedure to determine the valence band maximum level. The inset show the electronic configuration induced by crystal-field splitting of octahedral O_h(1T') and D_{3h}(2H) MoS₂ phases.

The partially unoccupied states were investigated with S *K*-edge NEXAFS spectroscopy. Figure 7 shows the S *K*-edge NEXAFS spectra of MoS₂-rGO and MoS₂-rGO-AuNPs nanocomposites. The MoS₂-rGO NEXAFS spectrum shows two main peaks below the sulfur ionization energy. Peak 2 (2471 eV) at resonance maximum can be attributed, according to previous reports, [63-65] to electronic transitions from the S1s core level to unoccupied hybridized S3p-Mo4d electronic states. The pre-edge shoulder at 2468.5 eV (peak 1) can be associated with the presence of S-O bond species [52,60,66]. A third peak, located at 2472.1 eV and attributed to S1s-3p_z electronic transitions has been observed for the MoS₂ monolayer sample (black line spectrum in Figure 7) showed here as comparison [63,65]. However, peak 3 is poorly defined in the NEXAFS spectra of MoS₂-rGO and MoS₂-rGO-AuNPs nanocomposites. According to

Guay et al., the energy separation between $S3p_{x,y}$ and $S3p_z$ electronic states is due to the difference of their symmetric properties at symmetry points Γ and A of the Brillouin zone for the 2H-MoS₂ phase [65]. Considering the Mo3d XPS results we saw that MoS₂-rGO nanocomposites are a mixture between 2H-MoS₂ and 1T'-MoS₂ phases, then, the presence of 1T'-MoS₂ metallic phase changes the symmetry properties of $S2p$ electronic states and reduces the energy separation between $S3p_{x,y}$ and $S3p_z$.

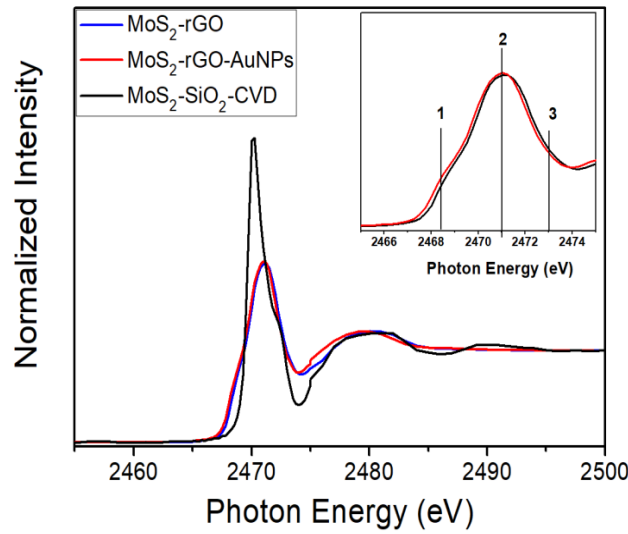


Figure 7. S K -edge NEXAFS spectra of MoS₂-rGO (blue solid line) and MoS₂-rGO-AuNPs (red solid line) nanocomposites. The S K -edge NEXAFS spectrum of the MoS₂ monolayer obtained by CVD [63] (black line) is also shown for the purpose of comparison. The inset shows a zoom of the first resonance peak. The numbers indicate the photon energies used to obtain the S-K $L_{2,3}L_{2,3}$ RAS spectra.

The degree of delocalization or electronic coupling between unoccupied electronic states is investigated by the core hole clock approach using S-K $L_{2,3}L_{2,3}$ RAS spectra. A detailed explanation about core hole clock method can be found elsewhere [67, 68] and is summarized in the supporting information file (SI). In this approach, the charge transfer times, used as a quantitative measure of electronic coupling (lower charge transfer time means high electronic coupling), are determined using lifetime

($\tau_{CH}=1.27$ fs in the case of the S *K*-edge [69]) of the core electron hole as an internal reference clock by:

$$\tau_{CT}=(I_{Raman}/I_{CT-Auger})\times \tau_{CH},$$

where I_{Raman} and $I_{CT-Auger}$ represent the intensities of different core-hole decay channels achieved by S-K $L_{2,3}L_{2,3}$ RAS spectroscopy. The “Raman” and “CT-Auger” electron decay channels correspond to different electronic final states. Raman decay correspond to the spectator two hole and one electron final states (2h1e) where the excited electron does not participate in the decay process. The second CT-Auger decay process consists of two holes (2h) in the valence band, reached when the electron is transferred out of the atom during the core-hole lifetime. S-K $L_{2,3}L_{2,3}$ RAS spectra shown in Figure 8 are convoluted by these core-decay channels. The attribution of “Raman” and “CT-Auger” decay channels in the RAS spectra is based on their behavior when the incident photon energy is tuned across the core excitation resonance. In Raman decay channels, the kinetic energy of the emitted electron increases when the energy of an incident photon is tuned across the resonance, while the CT-Auger contribution keeps at constant kinetic energy independently of the energy of the incident photon. The identification of the Raman and CT-Auger contributions forming the S-K $L_{2,3}L_{2,3}$ RAS spectra for MoS₂ was reported recently by Garcia-Basabe et al [63]. According to the last mentioned behavior of the “Raman” and “CT-Auger” decay channels (showed in Figure S5), we identified two spectators (blue and green in Figure 8) and one CT-Auger (red) contributions.

In this way, we determined τ_{CT} for S-K $L_{2,3}L_{2,3}$ RAS spectra obtained at photon energies labelled as 1 (2468.5 eV), 2 (2471 eV) and 3 (2472.1 eV) in the inset of Figure 7. The excitation of an electron to an unoccupied electronic state in the pre-edge shoulder of the S1s resonance spectrum (labelled as 1 ($h\nu=2468.5$ eV)), the τ_{CT} of 5.38 ± 0.60 fs and 7.74 ± 0.70 fs were obtained for MoS₂-rGO and MoS₂-rGO-AuNPs

nanocomposites, respectively. The increase in the τ_{CT} value for this photon energy was due to a decrease of the CT-Auger contribution from 18% in MoS₂-rGO to 12% in MoS₂-rGO-AuNPs nanocomposite. On the other hand, for electrons excited to electronic states in the S *K*-edge resonance maximum (labelled as 2 ($h\nu=2471.0$ eV)) the contribution of CT-Auger decay channel decrease from 24% to 17%, while the SP1 decay channel increases from 56% to 64% after AuNPs decoration. Therefore, for excitation energy of 2471.0 eV the τ_{CT} increase from 3.67 ± 0.60 fs in the MoS₂-rGO to 5.52 ± 0.70 fs in the MoS₂-rGO-AuNPs nanocomposites. The increase of τ_{CT} observed in the MoS₂-rGO-AuNPs nanocomposite can be interpreted as a reduction of the metallic character of the MoS₂-rGO nanocomposite due to the AuNPs. However, for photon energies labelled as 3 ($h\nu=2472.1$ eV), the τ_{CT} are very similar for both nanocomposites, close to 2.90 fs. The last results mean that the AuNPs affects only the unoccupied electronic states near to the MoS₂-rGO Fermi level. Thus, the results obtained by the core hole clock approach are in agreement with Mo 3d XPs analysis, where a transformation from metallic to semiconductor character after AuNPs decoration was observed.

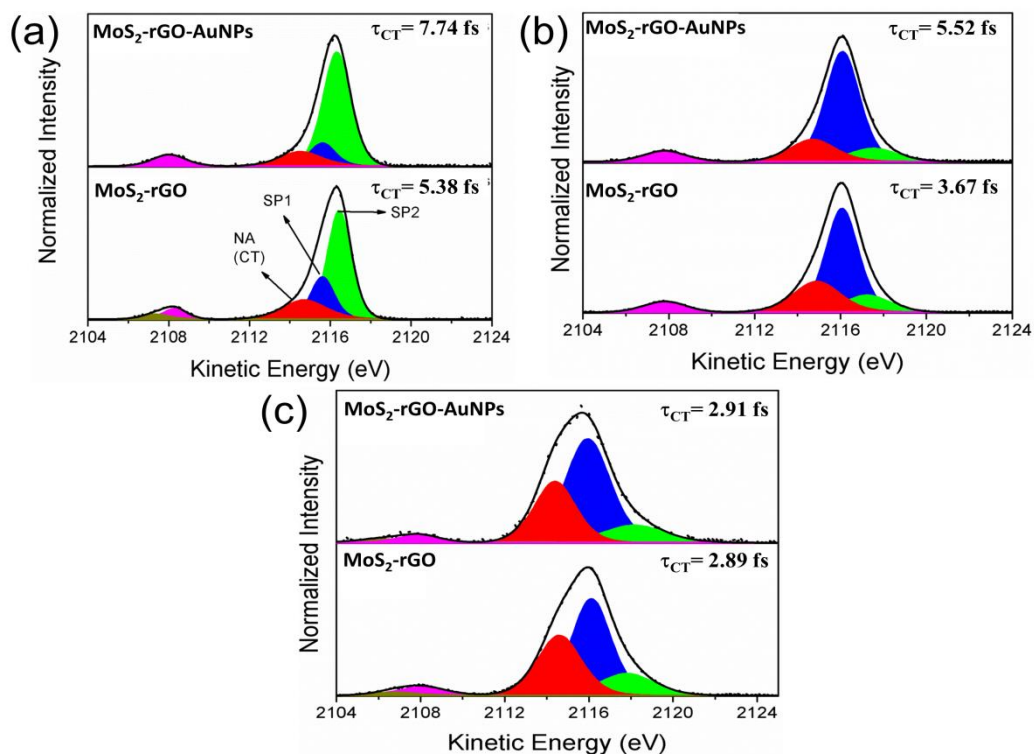


Figure 8. S-K $L_{2,3}L_{2,3}$ RAS spectra measured at photon energies labelled as 1-3 (2468.5 (a), 2471(b) and 2472.1 eV (c), respectively) in S K -edge NEXAFS spectrum. RAS spectra deconvolution in Raman spectators (blue - SP1 and green - SP2) and CT (red) decay channel are also showed.

4. CONCLUSION

In summary, we propose a simple approach to transform the MoS₂ from metallic to semiconductor character by AuNPs surface decoration in the solvothermal synthesized MoS₂-rGO nanocomposite. The AuNPs induces a p-type doping in MoS₂-rGO nanocomposite and reduce the stability of 1T' phase favoring the transformation to 2H-MoS₂. The main mechanism for this phase transition was electron transfer from 1T' Mo 4d_{xy,xz,yz} electronic states to AuNPs conduction band. The unoccupied electronic structure is also affected by AuNPs decoration, showing a strong electronic coupling between AuNPs and MoS₂ states close to the Fermi level. Our results suggest a practical method to modulate metallic and semiconductor character of MoS₂ phases in MoS₂-rGO nanocomposite.

ASSOCIATED CONTENT

Supporting Information

The SEM images and EDX spectra collected at different points in the MoS₂-rGO and MoS₂-rGO-AuNPs nanocomposites, Au 4f HRXPS spectrum of MoS₂-rGO-AuNPs nanocomposite, fitting parameters obtained from C1s, O1s, S2p and Mo3d high resolution spectra deconvolution for the MoS₂-rGO and MoS₂-rGO-AuNPs nanocomposites, band structure projected on orbitals of the different constituents for the isolated (2H-MoS₂ and Au (111)) structures and the composite material, Core Hole Clock Approach description section and photon energy dependence of electron kinetic energy of Resonant Auger decay channels.

ACKNOWLEDGEMENTS

Y. Garcia-Basabe acknowledges to CNPq for financial support (project (n°408265/2016-7). Research partially supported by LNLS – National Synchrotron Light Laboratory (SXS-20160596) and by CNPEM-LNNano (XPS-21999), Brazil. A.R.R. acknowledges financial support from CNPq and FAPESP (Project n° 2012/50259-8) and the Simons Foundation through the ICTP Associateship program. Theoretical calculations were carried out in the Scientific Computing Center at UNESP (NCC-Unesp), and in the Santos Dumont Supercomputer (LNCC-Santos Dumont). D. Grasseschi acknowledges to FAPESP for the financial support (grant no. 2015/10405-3).

References

- [1] Chhowalla, M., Liu, Z., Zhang, H. (2015) Two-dimensional transition metal dichalcogenide (TMD) nanosheets *Chem. Soc. Rev.* **44** 2584-2586.
- [2] Choi, W., Choudhary, N., Han, G.H., Park, J., Akinwande, D., Lee, Y.H. (2017) Recent development of two-dimensional transition metal dichalcogenides and their applications. *Mater Today* **20** 116-129.
- [3] Lv, R., Robison, J.A., Schaak, R.E., Sun, D., Y., S., Mallouk, T.E., Terrones, M. (2015) Transition metal dichalcogenides and beyond: synthesis, properties, and applications of single- and few-layer nanosheets. *Acc. Chem. Res.* **48** 56-64.
- [4] Barua, S., Dutta, H.S., Gogoi, S., Devi, R., Khan, R. (2018) Nanostructured MoS₂-Based Advanced Biosensors: A Review. *ACS Appl. Nano Mater.* **1** 2–25.
- [5] Zhang, G., Liu, H., Qu, J., Li, J. (2016) Two-dimensional layered MoS₂: rational design, properties and electrochemical applications *Energy Environ. Sci.* **9** 1190-1209
- [6] Kan, M., Wang, J.Y., Li, X.W., Zhang, S.H., Li, Y.W., Kawazoe, Y., Sun, Q., Jena, P. (2014) Structures and Phase Transition of a MoS₂ Monolayer. *J. Phys. Chem. C* **118** 1515-1522.
- [7] Yu, Y., Nam, G.H., He, Q., Wu, X.J., Zhang, K., Yang, Z., Chen, J., Ma, Q., Zhao, M., Liu, Z., Ran, F.-R., Wang, X., Li, H., Huang, X., Li, B., Xiong, Q., Zhang, Q., Liu, Z., Gu, L., Du, Y., Huang, W., Zhang, H. (2018) High phase-purity 1T'-MoS₂- and 1T'-MoSe₂-layered crystals. *Nat. Chem.* **10** 638–643.
- [8] Mak, K.F., Lee, C.H., Hone, J., Shan, J., Heinz, T.F. (2010) Atomically thin MoS₂: a new direct-gap semiconductor. *Phys. Rev. Lett.* **105** 136805.
- [9] Wypych, F., Schöllhorn, R. (1992) 1T-MoS₂, a new metallic modification of molybdenum disulfide *J. Chem. Soc., Chem. Commun.* **19** 1386-1388
- [10] Eda, G., Yamaguchi, H., Voiry, D., Fujita, T., Chen, M., Chhowalla, M. (2011) Photoluminescence from Chemically Exfoliated MoS₂. *Nano Lett* **11** 5111-5116.
- [11] Kappera, K., Voiry, D., Yalcin, S.E., Branch, B., Gupta, G., Mohite, A.D., Chhowalla, M. (2014) Phase-engineered low-resistance contacts for ultrathin MoS₂ transistors. *Nat. Mater.* **13** 1128–1134.
- [12] Scalise, E., Houssa, M., Pourtois, G., Afanas ev, V., Stesmans, A. (2012) Strain-Induced Semiconductor to Metal Transition in the Two-Dimensional Honeycomb Structure of MoS₂. *Nano Res.* **5** 43-48.

- [13] Radisavljevic, B., Radenovic, A., Brivio, J., Giacometti, V., Kis, A. (2011) Single-layer MoS₂ transistors. *Nat. Nanotech.* **6** 147–150.
- [14] Tsai, M.-L., Su, S.-H., Chang, J.-K., Tsai, D.-S., Chen, C.-H., Wu, C.-I., Li, L.-J., Chen, L.-J., He, J.-H. (2014) Monolayer MoS₂ Heterojunction Solar Cells. *ACS Nano* **8** 8317–8322.
- [15] Wang, Q.H., Kalantar-Zadeh, K., Kis, A., Coleman, J.N., Strano, M.S. (2012) Electronics and optoelectronics of two-dimensional transition metal dichalcogenides. *Nature Nanotech.* **7** 699-712
- [16] Chekin, F., Boukherroub, R., Szunerits, S. (2017) MoS₂/reduced graphene oxide nanocomposite for sensitive sensing of cysteamine in presence of uric acid in human plasma. *Mater. Sci. Eng., C* **73** 627–632.
- [17] Chekin, F., Teodorescu, F., Coffinier, Y., Pan, G.-H., Barras, A., Boukherroub, R., Szunerits, S. (2016) MoS₂/reduced graphene oxide as active hybrid material for the electrochemical detection of folic acid in human serum. *Biosens. Bioelectron.* **85** 807–813
- [18] Wang, R., Gao, S., Wang, K., Zhou, M., Cheng, S., Jiang, K. (2017) MoS₂@rGO Nanoflakes as High performance Anode Materials in Sodium ion Batteries. *Sci. Rep.* **7** 7963.
- [19] Xiang, Q., Yu, J., Jaroniec, M. (2012) Synergetic Effect of MoS₂ and Graphene as Cocatalysts for Enhanced Photocatalytic H₂ Production Activity of TiO₂ Nanoparticles. *J. Am. Chem. Soc.* **134** 6575-6578
- [20] Zhao, Y., Zhang, X., Wang, C., Zhao, Y., Zhou, H., Li, J., Jin, H. (2017) The synthesis of hierarchical nanostructured MoS₂/Graphene composites with enhanced visible-light photo-degradation property. *Appl. Surf. Sci.* **412** 207-213.
- [21] Meng, F., Li, J., Cushing, S.K., Zhi, M., Wu, N. (2013) Solar Hydrogen Generation by Nanoscale p–n Junction of p-type Molybdenum Disulfide/n-type Nitrogen-Doped Reduced Graphene Oxide. *J. Am. Chem. Soc.* **135** 10286–10289.
- [22] Ren, X., Ren, X., Pang, L., Zhang, Y., Ma, Q., Fan, H., Liu, S.F. (2016) MoS₂/sulfur and nitrogen co-doped reduced graphene oxide nanocomposite for enhanced electrocatalytic hydrogen evolution. *Int. J. Hydrogen Energy* **41** 916-923
- [23] Bai, L., Cai, X., Lu, J., Li, L., Zhong, S., Wu, L., Gong, P., Chen, J., Bai, S. (2018) Surface and Interface Engineering in Ag₂S@MoS₂ Core–Shell Nanowire Heterojunctions for Enhanced Visible Photocatalytic Hydrogen Production. *ChemCatChem* **10** 2107 –2114

- [24] Choi, M., Koppala, S.K., Yoon, D., Hwang, J., Kim, S.M. (2016) A route to synthesis molybdenum disulfide-reduced graphene oxide (MoS₂-RGO) composites using supercritical methanol and their enhanced electrochemical performance for Li-ion batteries. *J Power Sources* **309** 202-211.
- [25] Li, X., Li, J., Zhou, X., Ma, Y., Zheng, Z., Duan, X., Qu, Y. (2014) Silver nanoparticles protected by monolayer graphene as a stabilized substrate for surface enhanced Raman spectroscopy. *Carbon* **66**: 713-719.
- [26] Zhang, S., Wang, L., Zeng, Y., Xu, Y., Tang, Y., Luo, S., Liu, Y., Liu, C. (2016) CdS-Nanoparticles-Decorated Perpendicular Hybrid of MoS₂ and N-Doped Graphene Nanosheets for Omnidirectional Enhancement of Photocatalytic Hydrogen Evolution *ChemCatChem* **8** 2557-2564.
- [27] Huang, X., Zhen, Z., Bao, S., Wang, M., Qi, X., Fan, Z., Zhang, H. (2013) Solution-phase epitaxial growth of noble metal nanostructures on dispersible single-layer molybdenum disulfide nanosheets. *Nat Commun* **4** 1444.
- [28] Shi, Y., Huang, J.-K., Jin, L., Hsu, Y.-T., Yu, S., F., Li, L.-J., Yang, H.Y. (2013) Selective Decoration of Au Nanoparticles on Monolayer MoS₂ Single Crystals. *Sci. Rep.* **3** 1839.
- [29] Yin, Z., Chen, B., Bosman, M., Cao, X., Chen, J., Zheng, B., Zhang, H. (2014) Au Nanoparticle-Modified MoS₂ Nanosheet-Based Photoelectrochemical Cells for Water Splitting. *small* **10** 3537–3543.
- [30] Cho, Y., Sohn, A., Kim, S., Hahm, M.G., Kim, D.-H., Cho, B., Kim, D.-W. (2016) Influence of Gas Adsorption and Gold Nanoparticles on the Electrical Properties of CVD-Grown MoS₂ Thin Films. *ACS Appl. Mater. Interfaces* **8** 21612–21617.
- [31] Sreeprasad, T.S., Nguyen, P., Kim, N., Berry, V. (2013) Controlled, Defect-Guided, Metal-Nanoparticle Incorporation onto MoS₂ via Chemical and Microwave Routes: Electrical, Thermal, and Structural Properties. *Nano Lett.* **13** 4434–4441.
- [32] Grasseschi, D., Ando, R.A., Toma, H.E., Zamarion, V.M. (2015) Unraveling the nature of Turkevich gold nanoparticles: the unexpected role of the dicarboxyketone species. *RSC Adv.* **5** 5716–5724
- [33] Abbate, M., Vicentin, F.C., Compagnon-Cailhol, V., Rocha, M.C., Tolentino, H. (1999) The Soft X-ray Spectroscopy Beamline at the LNLS: Technical Description and Commissioning Results. *J. Synchrotron Radiat.* **6** 964–972.
- [34] Hohenberg, P., Kohn, W. (1964) Inhomogeneous electron gas. *Phys. Rev.* **136** B864-B871.

- [35] Kohn, W., Sham, L.J. (1965) Self-consistent equations including exchange and correlation effects. *Phys. Rev.* **140** A1133-1138.
- [36] Perdew, J.P., Burke, K., Ernzerhof, M. (1996) Generalized gradient approximation made simple. *Phys.Rev.Lett.* **77** 3865-3868.
- [37] Giannozzi, P., Baroni, S., Bonini, N., Calandra, M., Car, R., Cavazzoni, C., Ceresoli, D., Chiarotti, G.L., Cococcioni, M., Dabo, I. (2009) QUANTUM ESPRESSO: a modular and open-source software project for quantum simulations of materials. *J. Phys.: Condens. Matter* **21** 395502.
- [38] Tkatchenko, A., Scheffler, M. (2009) Accurate Molecular Van Der Waals Interactions from Ground-State Electron Density and Free-Atom Reference Data. *Phys. Rev. Lett.* **102** 073005.
- [39] Zhou, Y., Kiriya, D., Haller, E.E., Ager III, J.W., Javey, A., Chrzan, D.C. (2016) Compliant substrate epitaxy: Au on MoS₂. *Phys. Rev. B* **93** 054106.
- [40] Bruix, A., Miwa, J.A., Hauptmann, N., Wegner, D., Ulstrup, S., Grønborg, S.S., E., S.C., Dendzik, M., Cabo, A.G., Bianchi, M., Lauritsen, J.V., Khajetoorians, A.A., Hammer, B., Hofmann, P. (2016) Single-layer MoS₂ on Au (111): Band gap renormalization and substrate interaction. *Phys. Rev. B* **93** 165422.
- [41] Yan, Z., Chen, L., Yoon, M., Kumar, S. (2016) The Role of Interfacial Electronic Properties on Phonon Transport in Two-Dimensional MoS₂ on Metal Substrates. *ACS Appl. Mater. Interfaces* **8** 33299-33306.
- [42] Ferrari, A.C. (2007) Raman spectroscopy of graphene and graphite: Disorder, electron–phonon coupling, doping and nonadiabatic effects. *Solid State Commun.* **143** 47-57.
- [43] Cheng, C.-K., Lin, C.-H., Wu, H.-C., Ma, C.C.M., Yeh, T.-K., Chou, H.-Y., Tsai, C.-H., Hsieh, C.-K. (2016) The Two-Dimensional Nanocomposite of Molybdenum Disulfide and Nitrogen-Doped Graphene Oxide for Efficient Counter Electrode of Dye-Sensitized Solar Cells. *Nanoscale Res Lett* **11** 117.
- [44] Windom, B.C., Sawyer, W.C., Hahn, D.W. (2011) A Raman Spectroscopic Study of MoS₂ and MoO₃: Applications to Tribological Systems. *Tribol Lett* **42** 301–310.
- [45] Lee, C., Yan, H., Brus, L.E., Heinz, T.F., Hone, J., Ryu, S. (2010) Anomalous Lattice Vibrations of Single-and Few-Layer MoS₂. *ACS Nano* **4** 2695–2700.

- [46] Chakraborty, B., Bera, A., Muthu, D.V.S., Bhowmick, S., Waghmare, U.V., Sood, A.K. (2012) Symmetry-dependent phonon renormalization in monolayer MoS₂ transistor. *Phys. Rev. B* **85** 161403.
- [47] Wang, S., Zhang, D., Li, B., Zhang, C., Du, Z., Yin, H., Bi, X., Yang, S. (2018) Ultrastable In-Plane 1T–2H MoS₂ Heterostructures for Enhanced Hydrogen Evolution Reaction. *Adv. Energy Mater.* **8** 1801345.
- [48] Jeffery, A.A., Rao, S.R., Rajamathi, M. (2017) MoS₂–reduced graphene oxide (rGO) hybrid paper for catalytic applications by simple exfoliation–costacking. *Carbon* **112** 8-16.
- [49] Wu, P., Yin, N., Li, P., Cheng, W., Huang, M. (2017) Adsorption and diffusion behaviors of noble metal adatoms (Pd, Pt, Cu, Ag and Au) on MoS₂ monolayer: a first-principles study. *Phys. Chem. Chem. Phys.* **19** 20713-20722.
- [50] Ju, W., Li, T., Su, X., Li, H., Li, X., Ma, D. (2017) Au clusters adsorption on the perfect and the defective MoS₂ monolayers: structural and electronic properties. *Phys. Chem. Chem. Phys.* **19** 20735-20748.
- [51] Ambrosi, A., Sofer, Z., Pumera, M. (2015) 2H→1T phase transition and hydrogen evolution activity of MoS₂, MoSe₂, WS₂ and WSe₂ strongly depends on the MX₂ composition. *Chem. Commun.* **51** 8450-8453
- [52] Cai, L., He, J., Liu, Q., Yao, T., Yan, W., Hu, F., Jiang, Y., Zhao, Y., Hu, T., Sun, Z., Wei, S. (2015) Vacancy-Induced Ferromagnetism of MoS₂ Nanosheets. *J. Am. Chem. Soc.* **137** 2622–2627.
- [53] Dai, X., Du, K., Li, Z., Sun, H., Yang, Y., Zhang, W., Zhang, X. (2015) Enhanced hydrogen evolution reaction on few layer MoS₂ nanosheet seacoated functionalized carbon nanotubes. *Int. J. Hydrogen Energy* **40** 8877-8888
- [54] Chhowalla, M., Shin, H.S., Eda, G., Li, L.-J., Loh, K.P., Zhang, H. (2013) The chemistry of two-dimensional layered transition metal dichalcogenide nanosheets. *Nat. Chem.* **5** 263-275.
- [55] Pandey, M., Bothra, P., Pati, S.K. (2016) Phase Transition of MoS₂ Bilayer Structures. *J. Phys. Chem. C* **12** 3776-3780.
- [56] Acerce, M., Voiry, D., Chhowalla, M. (2015) Metallic 1T phase MoS₂ nanosheets as supercapacitor electrode materials. *Nat. Nanotech.* **10** 313.
- [57] Fan, X., Xu, P., Zhou, D., Sun, Y., Li, Y.C., Nguyen, M.A.T., Terrones, M., Mallouk, T.E. (2015) Fast and Efficient Preparation of Exfoliated 2H MoS₂ Nanosheets

by Sonication-Assisted Lithium Intercalation and Infrared Laser-Induced 1T to 2H Phase Reversion. *Nano Lett* **15** 5956-5960.

[58] Gao, G., Jiao, Y., Ma, Y., Jiao, Y., Wacławik, E., Du, A. (2015) Charge Mediated Semiconducting-to-Metallic Phase Transition in Molybdenum Disulfide Monolayer and Hydrogen Evolution Reaction in New 1T' Phase. *J. Phys. Chem. C* **119** 13124–13128.

[59] Lin, L., Miao, N., Wen, Y., Zhang, S., Ghosez, P., Sun, Z., Allwood, D.A. (2016) Sulfur-depleted monolayered molybdenum disulfide nanocrystals for superelectrochemical hydrogen evolution reaction. *ACS Nano* **10** 8929-8937.

[60] Yang, S., Zhang, K., Wang, C., Zhang, Y., Chen, S., Wu, C., Vasileff, A., Qiao, S., Song, L. (2017) Hierarchical 1T-MoS₂ Nanotubular Structures for Enhanced Supercapacitive Performance. *J. Mater. Chem. A* **5** 23704-23711.

[61] Liang, K.S., Hughes, G.J., Chianelli, R.R. (1984) UPS investigation of poorly crystallized MoS₂. *J. Vac. Sci. Technol. A* **2** 991.

[62] Tao, J., Chai, J.W., Zhang, Z., Pan, J.S., Wang, J. (2014) The energy-band alignment at molybdenum disulfide and high-k dielectrics interfaces. *Appl. Phys. Lett.* **104** 232110.

[63] Garcia-Basabe, Y., Rocha, A.R., Vicentin, F.C., Villegas, C.E.P., Nascimento, R., Romani, E.C., de Oliveira, E.C., Fehine, G.J.M., Li, S., Eda, G., Larrude, D.G. (2017) Ultrafast charge transfer dynamics pathways in two-dimensional MoS₂–graphene heterostructures: a core-hole clock approach *Phys. Chem. Chem. Phys.* **19** 29954-29962.

[64] Li, D., Bancroft, G.M., Kasrai, M., Fleet, M.E., Feng, X.H., Tan, K.H. (1995) Polarized X-ray Absorption Spectra and Electronic Structure of Molybdenite (2H-MoS₂). *Phys Chem Minerals* **22** 123-128.

[65] Guay, D., Divigalpitiya, W.M.R., Bélanger, D., Feng, X.H. (1994) Chemical Bonding in Restacked Single-Layer MoS₂ by X-ray Absorption Spectroscopy. *Chem. Mater.* **6** 614-619.

[66] Yang, C.-Y., Chiu, K.-C., Chang, S.-J., Zhang, X.-Q., Liang, J.-Y., Chung, C.-S., Pan, H., Wu, J.-M., Tseng, Y.-C., Lee, Y.-H. (2016) Phase-driven magneto-electrical characteristics of single-layer MoS₂. *Nanoscale* **8** 5627-5633.

[67] Föhlisch, A., Feulner, P., Hennies, F., Fink, A., Menzel, D., Sanchez-Portal, D., Echenique, P.M., Würth, W. (2005) Direct observation of electron dynamics in the attosecond domain. *Nature* **436** 373-376.

- [68] Menzel, D. (2008) Ultrafast charge transfer at surfaces accessed by core electron spectroscopies. *Chem. Soc. Rev.* **37** 2212–2223.
- [69] Campbell, J.L., Papp, T. (2001) Widths of the Atomic K–N7 Levels. *Atomic Data and Nuclear Data Tables* **77** 1-56.